ORIGINAL ARTICLE

J Rhinol 2023;30(2):87-97 | https://doi.org/10.18787/jr.2023.00027 pISSN 1229-1498 / eISSN 2384-4361
www.j-rhinology.org

The Effects of Various Maxillary Sinus Antrostomy Techniques on Modifying the Ventilation and Air-Conditioning Characteristics of the Maxillary Sinus: A Numerical Study

Seung Cheol Han, MD[1], Yang Na, PhD[2], and Tae-Bin Won, MD, PhD[1]

[1]Department of Otorhinolaryngology-Head and Neck Surgery, Seoul National University Hospital, Seoul National University College of Medicine, Seoul, Republic of Korea
[2]Department of Mechanical Engineering, Konkuk University, Seoul, Republic of Korea

Background and Objectives: Endoscopic sinus surgery is commonly performed for maxillary sinus (MS) disease, and the surgical extent of the MS medial wall or ostium varies. We examined the effect of MS surgery on nasal airflow and air-conditioning using computational fluid dynamics in five nasal cavity numerical models.

Methods: Four types of unilateral virtual MS surgery were conducted on the right MS based on computed tomography images of a 49-year-old man with normal anatomy. The five models were as follows: baseline (normal), middle meatal antrostomy (MMA), MMA with inferior meatal antrostomy (MMA+IMA), mega-antrostomy (MEGA), and endoscopic medial maxillectomy (EMM). Virtual simulator software and a stereoscopic display with haptic device were used for virtual surgery. Meshing software and computer fluid dynamics software were used to generate meshes and analyze airflow.

Results: The MMA and MMA+IMA results were similar to the baseline model. However, EMM and MEGA exhibited some physiological changes. The amount of airflow moving into the MS was largest in the EMM model, followed by the MEGA model. The distributions of wall shear stress and surface water-vapor increased near the enlarged MS ostium in EMM and MEGA. Skewed airflow partition and different airflow rates between the operated and unoperated sites of the nose also changed the air-conditioning characteristics. EMM substantially reduced the relative humidity in the nasopharynx, and MEGA showed a smaller reduction.

Conclusion: Among four surgery techniques, EMM produced the largest increase in wall shear stress and surface water vapor flux on the posterior surface of the MS and the greatest deterioration in the nasal cavity's air-conditioning capacity. MEGA reduced the local airflow disturbance inside the MS and prevented excessive degeneration of the cavity's overall air-conditioning capacity. In conclusion, MEGA and modified EMM approaches have physiological advantages over EMM, while securing a sufficient spatial extent of resection for surgery.

Keywords: Computational fluid dynamics; Virtual surgery; Middle meatal antrostomy; Mega antrostomy; Endoscopic medial maxillectomy.

INTRODUCTION

Endoscopic sinus surgery is an effective surgical technique to treat severe chronic rhinosinusitis. For diseases involving the maxillary sinus (MS), enlargement of the primary MS ostium is usually required to access internal lesions, such as polyps or tumors. Adequate ostium enlargement is also required to achieve effective postoperative drainage from the MS. The resection extent of the ostium and medial wall of the MS depends on its size and the type and severity of disease. The most frequently used technique is middle meatal antrostomy (MMA), in which the maxillary ostium is simply enlarged, usually accompanied by uncinectomy. In cases requiring more extensive resection, surgeons may resort to more aggressive techniques. For example, MMA can be combined with an inferior meatal antrostomy (IMA). An even larger extent of excision on the medial wall of the MS can be achieved via mega-antrostomy (MEGA), which involves the region ranging from

Received: March 27, 2023 **Revised:** April 19, 2023
Accepted: April 21, 2023

Address for correspondence: Tae-Bin Won, MD, PhD, Department of Otorhinolaryngology, Seoul National University Hospital, Seoul National University College of Medicine, 103 Daehak-ro, Jongno-gu, Seoul 03080, Republic of Korea
Tel: +82-2-2072-4037, **Fax:** +82-2-745-2387, **E-mail:** binent@hanmail.net

the posterior half of the inferior turbinate to the nasal floor. For some severe MS tumors, a more invasive operation technique, endoscopic medial maxillectomy (EMM), which even includes the resection of a significant portion of the inferior turbinate, can be utilized.

Predicting the prognosis of surgery is important for choosing an appropriate treatment. Generally, rhinologists' major concerns are favorable recovery of the MS mucosa, non-recurrence of the symptom or disease, and the maintenance of MS patency. Among many endoscopic MS operations, in EMM, there are some postoperative morbidities related to nasal airflow, such as nasal dryness, continuous crusting, and paradoxical obstruction, which are typical symptoms of empty nose syndrome [1,2]. Even technically successful EMM can be accompanied by these unexpected physiological issues. This necessitates establishing a link between post-EMM airflow symptoms and objective measures of nasal airflow. For example, a changed air-conditioning capacity of the nasal cavity in EMM may lead to an excessive loss of mucus from the epithelial surface, potentially resulting in nasal crusting and dryness. This conjecture is further supported by the physiological findings that the anterior portion of the inferior turbinate plays an important role in conditioning inhaled air [3-7], considering the EMM's resection extent. To overcome the physiological disadvantages of EMM, modified EMM has been proposed as a less extensive resection approach [8]. During modified EMM, the MS is widely opened (with a much larger opening than in MMA or IMA), while the inferior turbinate and nasolacrimal duct are almost completely preserved. A pre-lacrimal approach can be included as a type of modified EMM in this regard. MEGA is also similar to modified EMM in terms of the region of resection. Although modified EMM has been used widely instead of EMM according to certain indications, its physiological advantages have not been clearly defined—instead, to the best of the authors' knowledge, these advantages have only been inferred or subjectively assessed.

Computational fluid dynamics (CFD) is an effective predictive tool for investigating nasal physiology. It has been used to study the airflow and air-conditioning characteristics in normal, asymptomatic nasal cavities [5-7,9-13]. Recent studies have also used CFD to study abnormal airflow in pathologic or operated states [14,15]. With recent advances in patient-specific virtual surgical environments (VSEs), cost-effective virtual manipulation of nasal anatomy has become realizable for surgical planning [16]. CFD has been further extended in combination with the VSE technique to predict the physiological outcomes of nasal surgery [17].

The main objective of the present study was to use CFD to investigate the effect of four different MS surgery techniques—1) MMA, 2) combined MMA and IMA (MMA+IMA), 3) MEGA, and 4) EMM—on modifying the nasal airflow and air-conditioning characteristics. Virtual surgery was used to generate nasal cavity models simulating the surgical techniques. Additionally, several objective measures of airflow and air-conditioning characteristics were compared, especially between EMM and MEGA, which represented the modified EMM technique.

METHODS

Patients

The study subject was a 49-year-old man with no history of previous sinus surgery. The study subject had no nasal symptoms such as nasal obstruction, rhinorrhea, sneezing, or itching. Before constructing a numerical model, two otolaryngologists reviewed his computed tomography (CT) scans for anatomical defects. Septal deviation was not found, and asymmetric mucosal swelling affected by the nasal cycle was not noted. In the absence of any notable anatomical and etiological defects of the nasal cavity, this subject's CT scan was chosen as a baseline model for the present study. The volume of the left and right MSs was approximately 2.53×10^{-5} m^3 and 2.78×10^{-5} m^3, respectively. This study was approved by the Institutional Review Board of Seoul National University Bundang Hospital (IRB No. B-2207-767-701). In addition, informed consent was obtained from the subject.

Construction of the nasal cavity model and virtual surgery

A numerical model of the baseline nasal cavity was constructed using CT scans (Siemens, Erlangen, Germany) of the study subject. The slice thickness of the CT images was 0.5 mm. In addition to the baseline model, four additional cavity models were constructed by performing different types of virtual operations to the right MS of the baseline model to simulate MMA, MMA+IMA, MEGA, and EMM. This virtual intervention procedure was performed manually using virtual simulator platform software (CardinalSim; https://med.stanford.edu/cardinalsim.html) and a stereoscopic display (ASUS, Taiwan) with a Geomagic Touch haptic device (3D Systems, Rock Hill, SC, USA) (Supplementary Fig. 1 in the online-only Data Supplement). The external features of the face were included in all cavity models to obtain more realistic inflow conditions through the nostrils [9]. Paranasal sinuses other than the MS were removed in the construction of the numerical cavity models under the assumption that their presence would not significantly change the airflow or thermodynamic conditions of the nasal airway [9,12,18]. The segmentation procedure was conducted using Mimics v24.0 software (Materialise, Leuven, Belgium). The output file of Mimics v24.0 in

the stereolithography format was further processed using Geomagic Wrap 2017 (3D Systems) to produce a three-dimensional computational volume model (Supplementary Fig. 2 in the online-only Data Supplement).

CFD methodology

Nasal airflow fields were investigated at a constant inspiratory flow rate of 250 mL/s, which is the average breathing rate of an adult at rest [19]. Many numerical studies have suggested that flow at this rate does not exhibit significant turbulent features [9,11,13]; thus, a laminar flow regime was assumed. This target airflow rate of 250 mL/s was obtained by adjusting the pressure at the outlet for each cavity model in the preliminary computations. Velocity field, temperature, and humidity distributions of the inhaled air were evaluated using ANSYS/Fluent 2021 R2 software (Canonsburg, PA, USA). By using the wall model applied by Chung and Na [13], a more realistic epithelial surface temperature distribution was obtained, thereby satisfying a commonly used constant temperature boundary condition [18]. The mass fraction of water vapor along the epithelial surface was evaluated with an assumption of 100% relative humidity (RH) using in-house code that was provided to the ANSYS/Fluent in the form of a user-defined function. The ambient conditions were assumed to be 25°C, 35% RH, and a stagnation pressure of 0 Pa.

Fluent Meshing 2021 R2 was used to generate approximately 5.2–5.3 million mesh elements consisting of both prism layers and a polyhedral mesh following our preliminary study on grid-independence, which indicated that approximately 5 million polyhedral mesh elements resolved the airflow fields reasonably. Seven prism layers were placed along the surface, with a growth ratio of 1.15. The mesh distribution in one representative plane is shown in Supplementary Fig. 2 (in the online-only Data Supplement). A second-order central differencing scheme was used for the spatial discretization of governing equations to reduce dissipative numerical errors. A coupled algorithm was adopted for the velocity-pressure coupling algorithm.

RESULTS

Streamline patterns and velocity distributions in the MS

In the absence of obvious nasal septal deviation, the airflow was almost evenly distributed between the left and right airways in the baseline model (right:left=128.4 mL/s:122.9 mL/s=51.1%:48.9%), as described in Table 1. As the extent of surgery in the right MS increased—that is, moving from the MMA model to the MMA+IMA, MEGA, and EMM models in order—the unilateral airflow rate through the right-side airway increased. Since the bilateral airflow rate was set to a constant value of 250 mL/s in the present study, the asymmetry in the airflow partition between the left and right airways increased with the extent of surgery.

The amount of airflow moving through the right MS also depended on the type of operation. In the baseline model with a normal primary ostium, approximately 1.5 mL/s (equivalent to 1.2% of the unilateral airflow through the right airway) passed through the right MS. In the MMA model, however, the airflow rate going through the right MS increased to 11.8 mL/s (equivalent to 9.0% of the unilateral airflow through the right airway) due to the enlargement of the cross-sectional area of the primary ostium. The amount of airflow passing through the MS further increased with more aggressive intervention techniques. That is, two additional operations, in the MMA+IMA and MEGA models, caused a higher airflow rate to pass through the MS (25.7–27.9 mL/s). These airflow rates correspond to 18.2%–21.2% of the airflow rate moving through the right-side airway. However, a drastic increase in the amount of airflow rate entering the right MS was noted in the EMM model, where approximately 63.6% of the unilateral airflow rate through the right airway was found to enter the right MS, suggesting that the ventilation of the right MS significantly increased compared to the other models (Table 1).

The streamline patterns shown in Fig. 1 qualitatively illustrate that the degree of ventilation of the MS also depended on the type of operation. While infiltration of the airflow into the right MS was negligibly small in the baseline model, weak

Table 1. Summary of airflow partition, the unilateral airflow rate, and the airflow rate through the right MS

	Baseline	MMA	MMA+IMA	MEGA	EMM
Airflow partition (%), R:L	51.1:48.9	52.2:47.8	52.3:47.7	56.3:43.7	64.1:35.9
Airflow rate through the right nostril (mL/s)	128.4	130.9	131.5	141.3	160.9
Airflow rate entering the right MS (mL/s)	1.5	11.8	27.9	25.7	102.4
Ratio of airflow rate entering the right MS to airflow rate in the right nostril (%)	1.2	9.0	21.2	18.2	63.6

Computational fluid dynamics results are shown for the airflow rate in the baseline, MMA, MMA+IMA, MEGA, and EMM models.
MS, maxillary sinus; MMA, middle meatal antrostomy; IMA, inferior meatal antrostomy; MEGA, mega-antrostomy; EMM, endoscopic medial maxillectomy; R, right; L, left

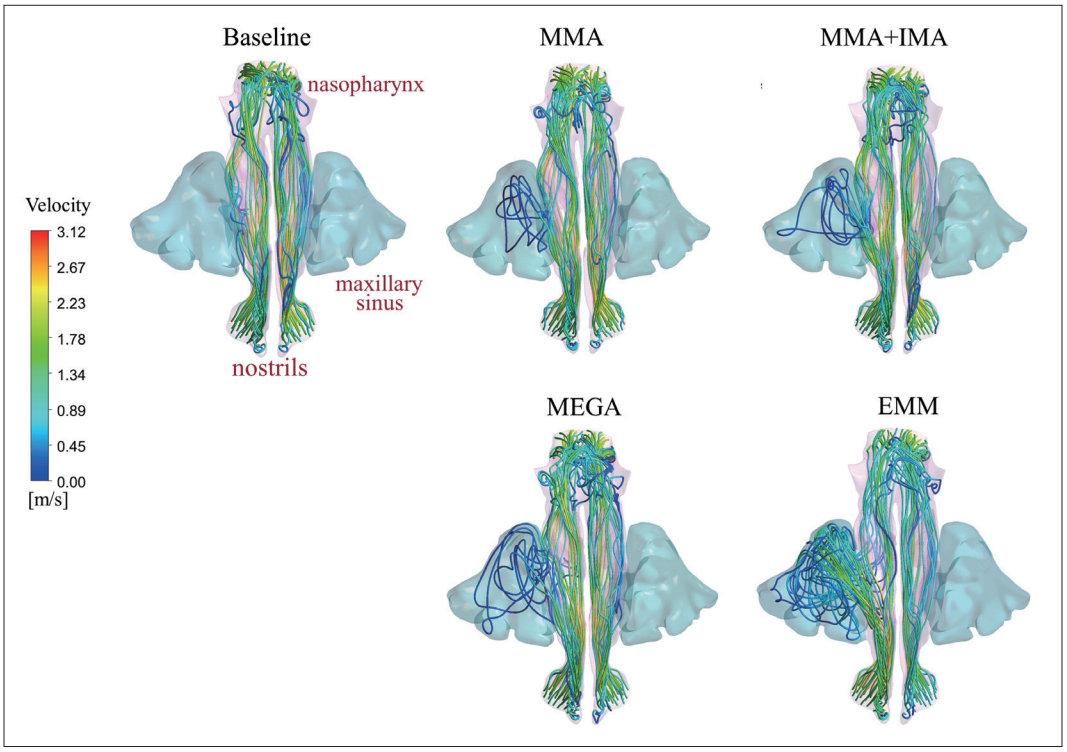

Fig. 1. Comparison of streamline patterns between five models. For visual convenience, the face was removed. Streamline patterns of airflow illustrate that the degree of ventilation of MS was different according to the operation technique. The infiltration of the airflow into the right MS was negligibly small in the baseline model. Weak permeation was observed in the MMA model, but limited to the region near the enlarged ostium. The degree of penetration of the airflow became even larger in the MMA+IMA and MEGA models. Complete penetration in the right MS was noted in the EMM model. MMA, middle meatal antrostomy; IMA, inferior meatal antrostomy; MEGA, mega-antrostomy; MS, maxillary sinus; EMM, endoscopic medial maxillectomy.

permeation was observed in the MMA model. However, the penetration of the airflow was limited to the region near the enlarged ostium. For more aggressive antrostomy techniques, such as in the MMA+IMA and MEGA models, the degree of penetration of the airflow became even larger compared to that of the MMA model. Complete penetration in the right MS was noted in the EMM model (Fig. 1).

The disturbance of the airflow inside the right MS caused by the different surgical techniques was also assessed by analyzing the velocity field inside the MS (Fig. 2). Five representative coronal planes were selected to show variations of the velocity field through the airway. The velocity inside the MS remained quite low (with a maximum velocity of less than 0.01 m/s) in the baseline model, indicating that the penetration of the airflow into the MS was negligibly small. Disturbed velocity fields in the right MS were noted in the MMA, MMA+IMA, and MEGA models, but penetration was limited to the region near the enlarged ostium or medial wall of the right MS. The maximum velocity near these regions was approximately 0.91, 1.42, and 0.82 m/s for the MMA, MMA+IMA, and MEGA models, respectively. In the MMA+IMA model, a higher maximum velocity of 1.42 m/s was found to occur near the lower airway passage connected to the inferior meatus. A drastically increased level of disturbance inside the right MS was observed in the EMM model, with a maximum velocity of 2.03 m/s near the extended ostium connected to the middle meatus.

RH and air temperature inside the MS

The RH and air temperature fields in the same representative coronal planes are compared in Supplementary Figs. 3 and 4 (in the online-only Data Supplement). Similar to the behavior of the velocity field shown in Fig. 2, the disturbance inside the MS was negligible in the baseline model; therefore, the RH inside the MS was almost undisturbed, maintaining a level of 100%. In the other three models (i.e., the MMA, MMA+IMA, and MEGA models), the average RH of the right MS was found to be over 97% (i.e., 99.7%, 97.4%, and 98.4% for the MMA, MMA+IMA, and MEGA models, respectively), consistent with the limited penetration of airflow into the right MS (Fig. 2). In the EMM model, however, the region affected by the airflow penetration spread over the entire volume of the right MS, and the resulting spatial average of the RH in the right MS dropped to 89.8% (Supplementary

Fig. 3 in the online-only Data Supplement).

Reflecting the similarity between the heat and water-vapor transport phenomena, the behaviors of the air temperature fields were shown to be quite similar to those of the RH fields. When the penetration of the airflow was minimal to modest, the average temperature was maintained at over 33°C in the right MS (i.e., 33.3°C, 33.1°C, and 33.0°C for the MMA, MMA+IMA, and MEGA models, respectively). However, when the highest level of airflow penetration into the MS occurred in the EMM model, the average temperature of the right MS dropped to 31.6°C (Supplementary Fig. 4 in the online-only Data Supplement).

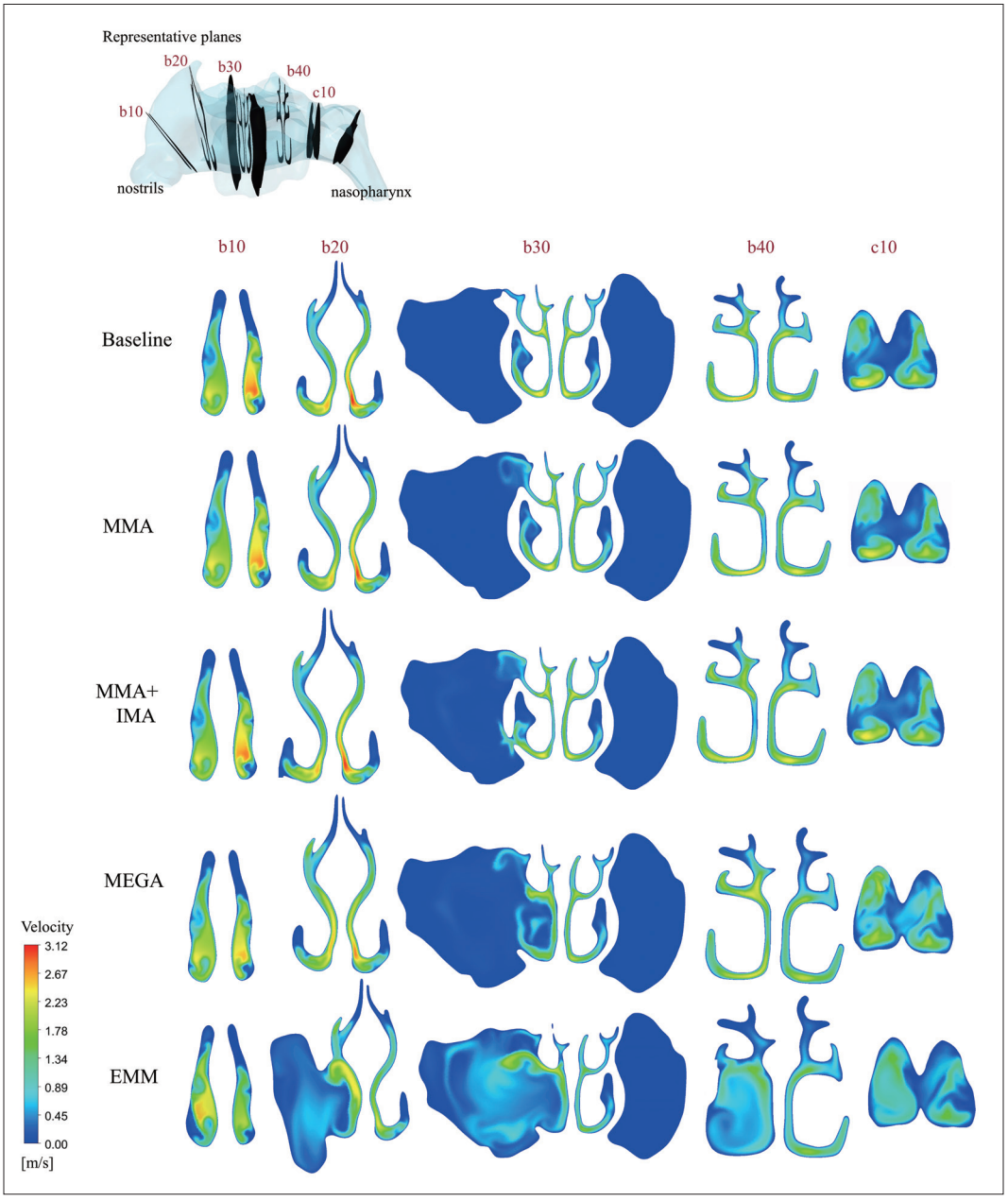

Fig. 2. Comparison of velocity distributions along the nasal airway in five representative coronal planes. The bilateral airflow velocity magnitude is shown by five representative planes from the anterior part to the posterior part. In the baseline model, the velocity inside the MS was very low, with a maximum velocity less than 0.01 m/s. However, disturbed velocity regions were found near the enlarged ostium or medial wall of the right MS in the MMA, MMA+IMA, and MEGA models, and the maximum velocity near these regions was approximately 0.91, 1.42, and 0.82 m/s in the MMA, MMA+IMA, and MEGA models, respectively. In the EMM model, a drastically increased level of disturbance inside the right MS was found, with a maximum velocity of 2.03 m/s near the extended ostium connected to the middle meatus. MS, maxillary sinus; MMA, middle meatal antrostomy; IMA, inferior meatal antrostomy; MEGA, mega-antrostomy; EMM, endoscopic medial maxillectomy.

Wall shear stress and epithelial surface water-vapor flux along the MS surface

The distribution of the wall shear stress along the surface of the nasal cavity is shown in Fig. 3. In a healthy normal nasal cavity, represented by the baseline model, the nasal valve area is subject to high wall shear stress due to the acceleration of the inhaled airflow. In fact, a maximum wall shear stress of approximately 0.494 Pa was observed in this region of the baseline model. In contrast, the significantly reduced velocity inside the MS (typically less than 0.01 m/s) resulted in vanishingly small wall shear stress along the epithelial surface of the MS (Fig. 3A).

Even when the airflow rate into the MS increased to 25.7 mL/s (equivalent to 18.2% of the unilateral airflow rate through the right airway) in the MEGA model, the wall shear stress at the surface of the right MS remained negligibly small (Fig. 3A). It is noteworthy, however, that the wall shear stress at the posterior surface of the enlarged ostium between the right nasal

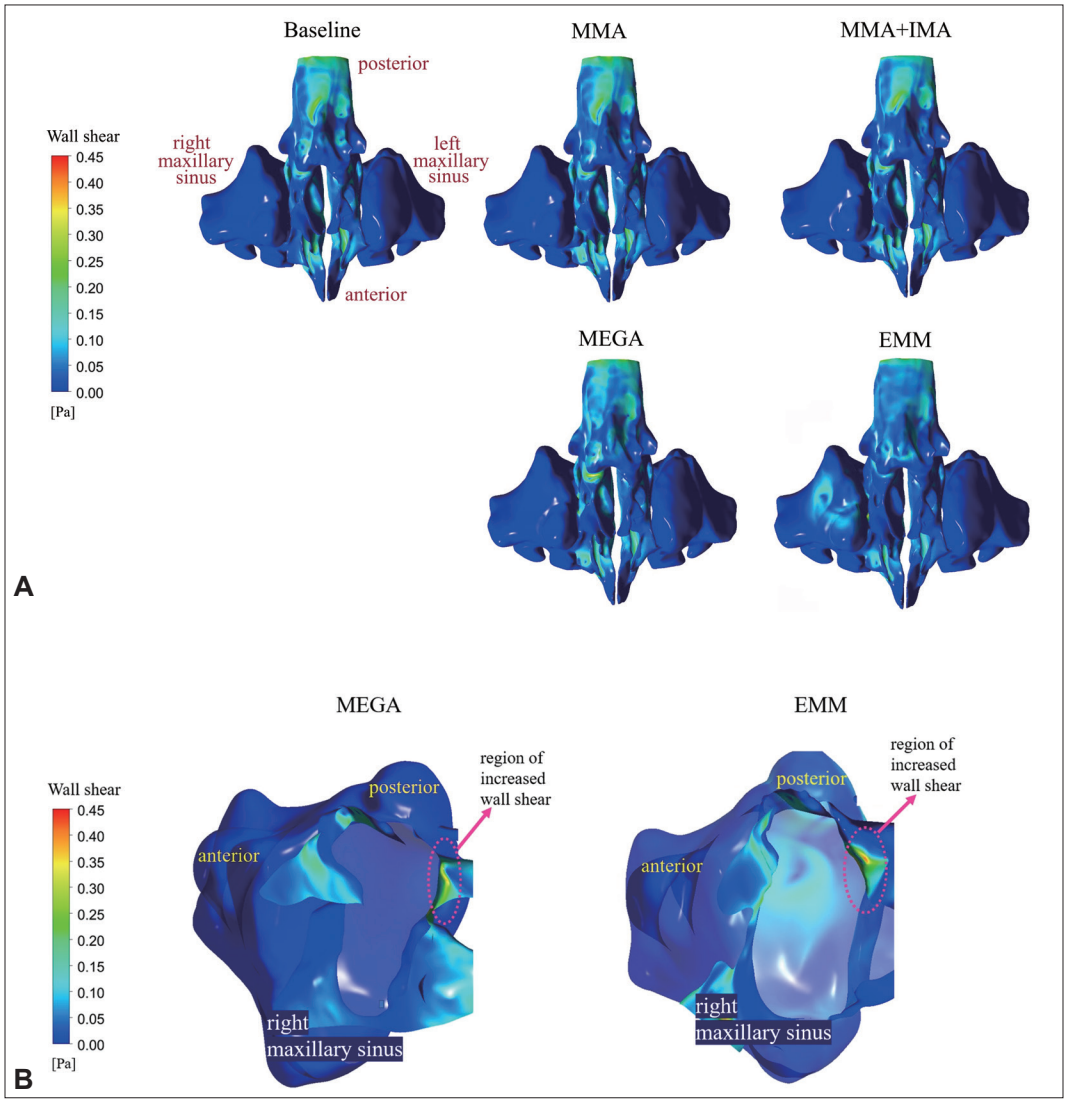

Fig. 3. Comparison of wall shear stress distributions between five models. A: Overall distribution of wall shear stress in five models. In the baseline model, the nasal valve area was subject to high wall shear stress, and a maximum wall shear stress of 0.494 Pa was observed. From the epithelial surface of the MS in the baseline model, vanishingly small wall shear stress was measured. In the MMA, MMA+IMA, and MEGA models, the wall shear stress at the surface of the right MS remained small. However, in the EMM model, a region exposed to elevated wall shear stress appeared at the posterior surface of the right MS. B: The distribution of wall shear stress near the extended ostium in the MEGA and EMM models. For visual purposes, the cavity connected to the right MS was artificially removed. In the MEGA model, the wall shear stress at the posterior surface of the enlarged ostium increased to approximately 0.364 Pa. In the EMM model, a higher value of wall shear stress (approximately 0.412 Pa) was noted in the posterior surface of the enlarged ostium. In addition, the EMM model showed increased wall shear stress (approximately 0.155 Pa) at the posterior surface of the right MS. MS, maxillary sinus; MMA, middle meatal antrostomy; IMA, inferior meatal antrostomy; MEGA, mega-antrostomy; EMM, endoscopic medial maxillectomy.

cavity and the MS increased to approximately 0.364 Pa in MEGA model (Fig. 3B). When the airflow rate into the right MS further increased to 102.4 mL/s (equivalent to 63.6% of the unilateral airflow rate through the right airway) in the EMM model, the flow kinematics inside the right MS completely changed; as a result, the posterior surface of the right MS was exposed to increased wall shear stress (approximately 0.155 Pa). It is a distinctive characteristic of the EMM model that the region exposed to the elevated wall shear stress appears at the posterior surface of the right MS. Furthermore, compared to the MEGA model, a higher value of wall shear stress (approximately 0.412 Pa) was noted on the posterior surface of the enlarged ostium between the right nasal cavity and the MS (Fig. 3B).

The distribution of water-vapor flux along the MS epithelial surface was also investigated (Fig. 4). Similar to the wall shear stress distributions, the disturbances produced by the airflow penetrating into the right MS did not cause a noticeable change in the water-vapor flux along the surface of the right MS in the MMA, MMA+IMA, and MEGA models. In the EMM model, however, elevated levels of water-vapor flux of approximately 1.60×10^{-3} kg/(s·m^2) occurred on the posterior surface of the right MS. This was due to the collision of a bulk of airflow entering from the right airway into the MS.

In order to understand the appearance of the region subject to an increased level of wall shear stress and water-vapor flux on the posterior surface of the right MS in the EMM model, the local flow field inside the right MS was further explored. As shown in Fig. 5, a large portion of the airflow originating from the right nostril entered the right MS. A bulk of the penetrating airflow proceeded before colliding with the posterior surface of the right MS. Therefore, a stagnation area formed on the posterior surface of the MS where the wall shear stress and the surface water-vapor flux increased.

Nasal resistance and post-choanal RH and air temperature

The overall effects of the different surgical techniques on the nasal airflow were estimated by analyzing the variations in the nasal resistance, RH, and air temperature in the nasopharynx (Table 2). Unilateral nasal resistance in the right-side airway decreased as the extent of surgery increased (from 0.0543 Pa·s/mL in the baseline model to 0.0269 Pa·s/mL in the EMM model). Bilateral nasal resistance also decreased similarly to the behavior of the unilateral nasal resistance in the right airway. In particular, the EMM model yielded the largest reduction in bilateral nasal resistance, by 37.5% from that of the baseline model (from 0.0277 Pa·s/mL to 0.0173 Pa·s/mL).

The RH and air temperature measured after the choanae are also compared in Table 2. Meaningful differences in the RH in the nasopharynx were not noted among the baseline, MMA, and MMA+IMA models. Even in the MEGA model, the decrease of RH from the normal baseline model may not

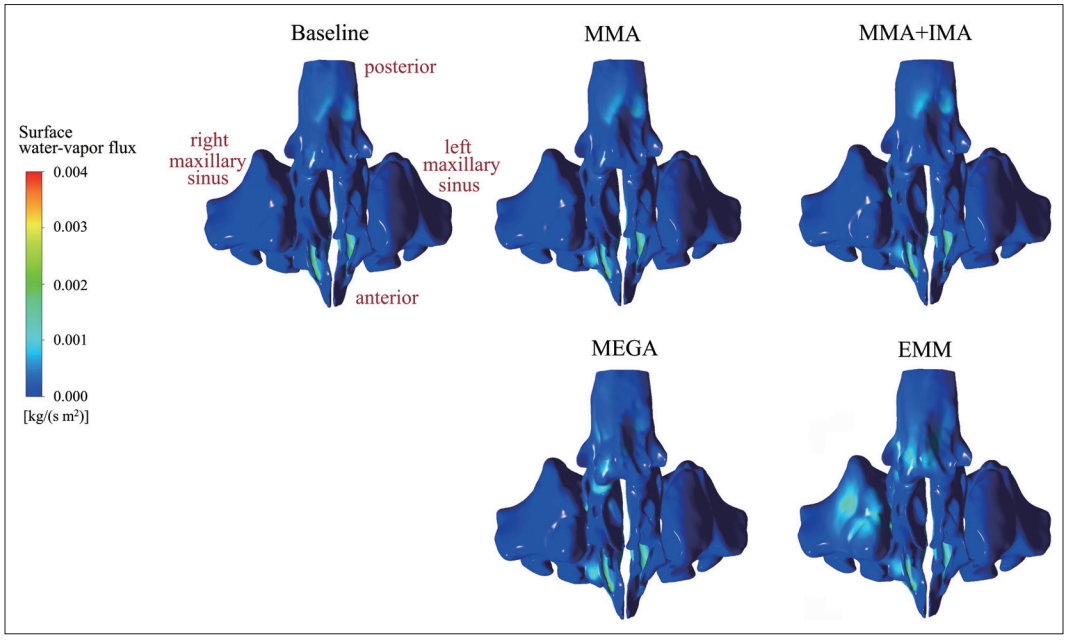

Fig. 4. Comparison of epithelial surface water-vapor flux distributions between five models. In the MMA, MMA+IMA, and MEGA models, there were no noticeable changes in water-vapor flux along the surface of the right MS. In the EMM model, however, the water-vapor flux on the posterior surface of the right MS increased to approximately 1.60×10^{-3} kg/(s·m^2). MMA, middle meatal antrostomy; IMA, inferior meatal antrostomy; MEGA, mega-antrostomy; MS, maxillary sinus; EMM, endoscopic medial maxillectomy.

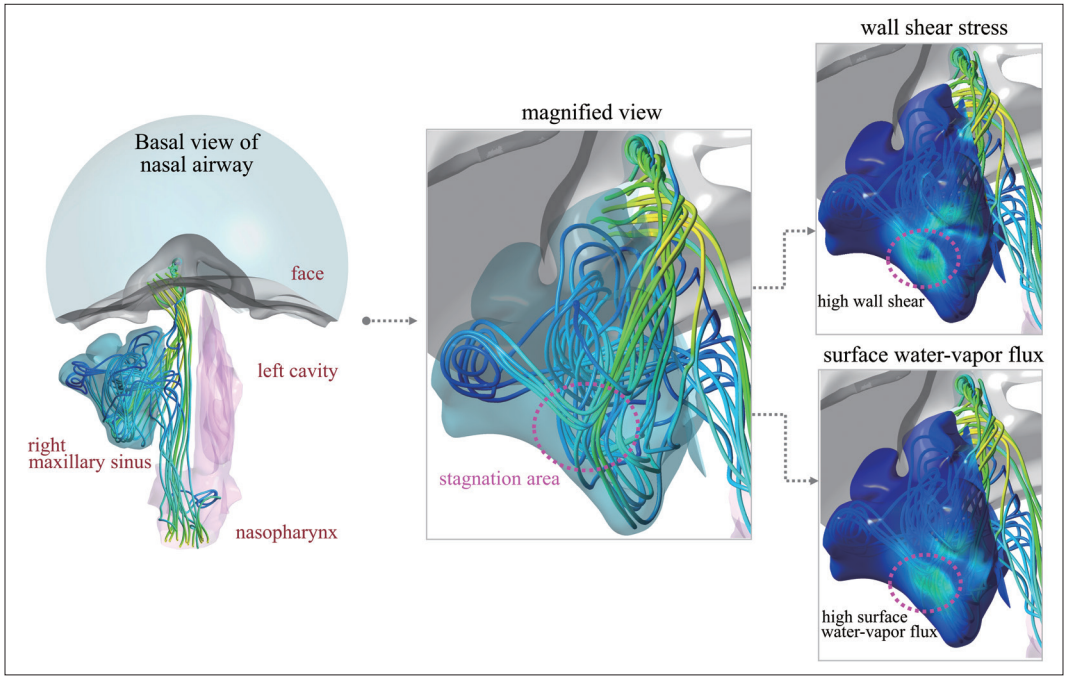

Fig. 5. Stagnation in the posterior surface of the maxillary sinus of the EMM model. A large portion of the airflow from the right nostril entered the right maxillary sinus. A bulk of penetrating airflow proceeded before colliding with the posterior surface of the right maxillary sinus. Therefore, a stagnation area was formed on the posterior surface of the maxillary sinus where the wall shear stress and surface water-vapor flux increased. For visual convenience, only the airflow through the right nasal cavity was considered and the surface of the right maxillary sinus was made semi-transparent. EMM, endoscopic medial maxillectomy.

Table 2. Summary of nasal resistance, relative humidity, and air temperature between four surgery models

	Baseline	MMA	MMA+IMA	MEGA	EMM
Unilateral nasal resistance (Pa·s/mL), R:L	0.0543:0.0565	0.0518:0.0563	0.0514:0.0557	0.0419:0.0532	0.0269:0.0484
Bilateral nasal resistance (Pa·s/mL)	0.0277	0.0268	0.0267	0.0234	0.0173
Relative humidity, before choanae (%), R:L	91.6:91.8	92.3:91.6	92.3:91.7	89.5:92.7	84.6:94.3
Relative humidity, after choanae (%)	91.7	92.3	92.1	91.0	88.1
Air temperature, before choanae (°C), R:L	31.9:31.9	32.0:31.9	32.0:31.9	31.6:32.1	31.2:32.4
Air temperature, after choanae (°C)	31.9	32.0	32.0	31.9	31.7

Computational fluid dynamics results are shown for the nasal resistance, relative humidity, and the air temperature. MMA, middle meatal antrostomy; IMA, inferior meatal antrostomy; MEGA, mega-antrostomy; EMM, endoscopic medial maxillectomy; R, right; L, left

have been physiologically significant (from 91.7% in the baseline model to 91.0% in the MEGA model). In the EMM model, however, the largest decrease in RH was noted (from 91.7% in the baseline model to 88.1% in the EMM model). The sizable reduction in the RH observed in the EMM model is attributable to the reduced air-conditioning capacity of the right airway. As shown in Table 1, the airflow partition between the right and left airways was highly skewed to the right side (R:L= 160.9 mL/s:90.1 mL/s); thus, the overloaded right airway was not able to condition the inhaled air sufficiently. Accordingly, the RH in the right airway just before the choanae was shown to drop to as low as 84.6% in the EMM model.

The behavior of air temperature was similar to that of RH, but with much less deviation. The air temperature in the nasopharynx did not meaningfully vary between the baseline, MMA, MMA+IMA, and MEGA models. Even in the EMM model, the reduction in air temperature was not significant (from 31.9°C in the baseline model to 31.7°C in the EMM model).

DISCUSSION

In this study, numerical models for nasal cavities simulating four different surgical techniques (MMA, MMA+IMA,

MEGA, and EMM) were generated using a virtual surgery technique and analyzed by CFD. The resulting airflow and air-conditioning characteristics were compared with those of a baseline model of the normal nasal cavity. Our results suggest that EMM involves an anatomical change that results in the largest increase of wall shear stress and surface water-vapor flux on the posterior surface of the MS and the greatest deterioration of air-conditioning characteristics in the nasal cavity. In contrast, the MEGA model, which we used to represent modified EMM, was shown to significantly reduce airflow penetration into the MS compared to the EMM model. As a result of reduced airflow disturbance in the nasal airway, the deterioration in the RH in the nasopharynx was quite reduced in the MEGA model. From this point of view, our study suggests that MEGA has a substantial advantage over EMM in terms of nasal physiology.

The MMA and MMA+IMA results of our study showed that there were minimal physiologic changes after surgery. However, EMM or MEGA led to some physiological changes. This is clearly due to the much greater extent of resection during the operation in the latter techniques. Therefore, our study further focused on the difference between MEGA and EMM, both of which remove a large portion of the medial wall of the MS. EMM's weak point is believed to be related to inferior turbinectomy. The inferior turbinate and anterior portion of the nasal cavity play an important role in properly conditioning the inhaled air [3-7]. Unlike EMM, MEGA extends the antrostomy through the posterior half of the inferior turbinate down to the nasal floor and thereby preserves the anterior end part of the inferior turbinate. The pre-lacrimal approach [8] is used in the modified EMM technique, and the inferior turbinate/maxillary medial complex is returned to its original anatomical status at the end of the procedure. Although the pre-lacrimal approach is more widely used than MEGA, MEGA is an older technique and has long been known as an effective and safe treatment option for recalcitrant or refractory MS disease [20,21]. Furthermore, MEGA is easier to virtually implement than pre-lacrimal approach because the pre-lacrimal approach includes a procedure for returning the inferior turbinate to its place after the MS operation. This is why we chose the MEGA model instead of the pre-lacrimal approach for representing the modified EMM technique. Objective criteria for comparing different surgical techniques have not been established. Thus, we compared MEGA and EMM in two key physiological aspects: 1) the outcome of increased airflow penetration into the MS and 2) the effect of airflow modification on the air-conditioning capacity.

Firstly, the disturbance inside the MS increased with the amount of airflow moving through the MS. The EMM model allowed the largest amount of airflow penetration into the MS (approximately 63.6% of the unilateral airflow through the right nostril), due to the sizable resection of the medial surface of the MS. Since a bulk of the airflow entering the MS proceeded directly toward the posterior surface of the MS before it hit the surface, a stagnation region was formed on the collision area. This is the region where local increases in wall shear stress and surface water-vapor flux were noted. The appearance of this local region near the posterior surface of the MS would be an unwanted outcome of EMM. The increased level of wall shear stress may induce local inflammatory symptoms by irritating the local epithelial surface. In addition, the increased level of surface water-vapor flux would lead to an excessive loss of mucus from the mucosal surface, thereby inducing postoperative symptoms such as dehydration or crust formation. In fact, crust formation has been described as a concern of large-scale antrostomy in previous studies [2,22]. In this context, by suppressing the elevated level of wall shear stress or surface water-vapor flux, the MEGA model is expected to reduce the local inflammatory symptoms or crust formation that EMM is likely to cause. This conjecture is further justified by several previous studies. For example, a study on 35 patients who underwent medial maxillectomy reported nasal crusting in all 35 patients [1]. However, another study about the pre-lacrimal approach in 51 patients showed no nasal crusting complications [23].

Another critical issue is the excessive ventilation of the MS observed in the EMM model. A significant increase in the airflow entering the right MS can lower the nitric oxide (NO) concentration inside the MS by excessive washout that is enhanced by an increased level of convective transport [10]. The low NO concentration inside the MS can aggravate the sanitary environment inside the MS. Although studies on the role of NO in the pathogenesis of sinus infection have not reported consistent findings, it is generally accepted that maintaining high NO concentrations is protective [24,25]. Consistent with our results, a postoperative decrease in NO concentrations inside the MS has also been reported [17,26]. In this respect, the protective role of NO inside the MS could be diminished to a greater extent after EMM compared to the other three techniques, including MEGA.

The second physiological measure for the comparison of surgery techniques has to do with the degree of deterioration in the air-conditioning capacity. EMM performed unilaterally to the right MS induced a highly skewed airflow partition between both airways. Therefore, the airflow rate moving through the right-side cavity increased by approximately 25% (from 128.4 mL/s in the baseline model to 160.9 mL/s in the EMM model). A recent study comparing the modified EMM and EMM by virtual surgery and CFD also showed that the conventional EMM model had higher velocity fields and a more

massive flow rate increase than the modified EMM model [27]. This is in line with our study's results. However, we further investigated the effect of increased airflow rate on RH and temperature. There was less difference in the air temperature of the nasopharynx than in RH. We think that this may be because the air temperature changes after the energy of the air humidity itself is consumed first. Nonetheless, there was a difference in the RH in the nasopharynx. The operated nasal cavity was not able to sufficiently condition the increased amount of air, resulting in an insufficient rise of RH. In the EMM model, a sizable reduction of RH in the nasopharynx was unavoidable because of the large increase in the amount of airflow by the skewed airflow partition (64.1%), combined with the deteriorated air-conditioning capacity resulting from the loss of the inferior turbinate. However, in the MEGA model, the decrease in the RH in the nasopharynx from the baseline model was much smaller than in the EMM model. This favorable result was attributed partly to the more balanced airflow partition through the operated-side cavity (approximately 56.3%) and partly to the benefit of preserving the physiological role of the inferior turbinate. This inference is based on the known role of the inferior turbinate and anterior portion of the cavity in conditioning the inhaled air [3-7].

From the viewpoint of nasal obstruction, it is interesting to note that nasal resistance (both unilateral and bilateral) was significantly reduced in the EMM model. Since the subject did not have any complaint of nasal obstruction at baseline, it can be inferred that the reduction of nasal resistance achieved after surgery would not further improve the short-term evaluation of the subjective sensation of patency. Although several studies have conjectured that patients' sensory perceptions and mucosal cooling may contribute to subjective measures of nasal obstruction [28-30], the level of RH and air temperature relative to the alveolar condition is also important for the long-term evaluation of subjective patency. In this context, the lowest level of RH in the nasopharynx is an inherent shortcoming of EMM.

Overall, our results indicate that MEGA provided several physiological advantages over EMM, justifying the increasing popularity of modified EMM or the pre-lacrimal approach in recent years. In MEGA, the deterioration in nasal anatomy appears to be in the acceptable range, so that excessive airflow disturbance inside the MS can be avoided. Additionally, the reduction in the air-conditioning capacity from the baseline model is minimized. Therefore, our results suggest that MEGA, which represents modified EMM, can be a good compromise between minimizing the disturbance of the physiological functions of the nasal cavity and achieving a sufficient resection extent.

Our study has several limitations. Since only one study subject was used, the present CFD results should be interpreted with caution. Additionally, a constant inspiratory airflow rate of 250 mL/s, which is an average airflow rate during inspiration, was considered; thus, the limitations of this steady-state assumption should also be noted. However, according to several studies [5,13], steady-state computation could reasonably represent the general features of the velocity and temperature fields during inspiration. Thus, we believe that our results suitably reveal the distinctive physiological features induced by four different surgery techniques applied to the MS.

The effects of four different MS surgical techniques on the nasal airflow and air-conditioning characteristics were investigated via CFD in this study. Numerical models for the nasal cavity simulating MMA, MMA+IMA, MEGA and EMM were generated by applying a virtual surgery technique to a healthy baseline subject. Among the four surgery techniques, EMM produced the largest increase in wall shear stress and surface water vapor flux on the posterior surface of the MS and the greatest deterioration in the air-conditioning capacity of the nasal cavity. MEGA, however, was shown to reduce the local airflow disturbance inside the MS and prevent excessive degeneration of the overall air-conditioning capacity of the cavity. In conclusion, MEGA or modified EMM approaches have physiological advantages over EMM while securing a sufficient spatial extent of resection for surgery.

Supplementary Materials

The online-only Data Supplement is available with this article at https://doi.org/10.18787/jr.2023.00027.

Availability of Data and Material

All data generated or analyzed during the study are included in this published article and its supplementary information files.

Conflicts of Interest

The authors have no potential conflicts of interest to disclose.

Author Contributions

Conceptualization: Tae-Bin Won. **Data curation:** Seung Cheol Han, Yang Na. **Formal analysis:** Seung Cheol Han. **Investigation:** Seung Cheol Han, Tae-Bin Won. **Methodology:** Seung Cheol Han, Yang Na. **Project administration:** Tae-Bin Won. **Resources:** Yang Na, Tae-Bin Won. **Software:** Yang Na. **Supervision:** Tae-Bin Won. **Validation:** Seung Cheol Han. **Visualization:** Yang Na. **Writing—original draft:** Seung Cheol Han. **Writing—review & editing:** Yang Na, Tae-Bin Won.

ORCID iDs

Seung Cheol Han https://orcid.org/0000-0003-1981-9334
Yang Na https://orcid.org/0000-0001-5729-6912
Tae-Bin Won https://orcid.org/0000-0003-2266-3975

Funding Statement

None

REFERENCES

1) Osguthorpe JD, Weisman RA. 'Medial maxillectomy' for lateral nasal wall neoplasms. Arch Otolaryngol Head Neck Surg 1991;117(7):751-6.
2) Kennedy DW, Adappa ND. Endoscopic maxillary antrostomy: not just a simple procedure. Laryngoscope 2011;121(10):2142-5.
3) Tan J, Han D, Wang J, Liu T, Wang T, Zang H, et al. Numerical simulation of normal nasal cavity airflow in Chinese adult: a computational flow dynamics model. Eur Arch Otorhinolaryngol 2012;269(3): 881-9.
4) Weber RK, Werner JA, Hildenbrand T. Endonasal endoscopic medial maxillectomy with preservation of the inferior turbinate. Am J Rhinol Allergy 2010;24(6):132-5.
5) Lindemann J, Keck T, Wiesmiller K, Sander B, Brambs HJ, Rettinger G, et al. Nasal air temperature and airflow during respiration in numerical simulation based on multislice computed tomography scan. Am J Rhinol 2006;20(2):219-23.
6) Garcia GJ, Bailie N, Martins DA, Kimbell JS. Atrophic rhinitis: a CFD study of air conditioning in the nasal cavity. J Appl Physiol (1985) 2007; 103(3):1082-92.
7) Kim DW, Chung SK, Na Y. Numerical study on the air conditioning characteristics of the human nasal cavity. Comput Biol Med 2017;86: 18-30.
8) Ashman A, Psaltis AJ, Wormald PJ, Tan NC. Extended endoscopic approaches to the maxillary sinus. J Laryngol Otol 2020;134(6):473-80.
9) Doorly DJ, Taylor DJ, Schroter RC. Mechanics of airflow in the human nasal airways. Respir Physiol Neurobiol 2008;163(1-3):100-10.
10) Chung SK, Jo G, Kim SK, Na Y. The effect of a middle meatal antrostomy on nitric oxide ventilation in the maxillary sinus. Respir Physiol Neurobiol 2014;192:7-16.
11) Burgos MA, Sanmiguel-Rojas E, Martín-Alcántara A, Hidalgo-Martínez M. Effects of the ambient temperature on the airflow across a Caucasian nasal cavity. Int J Numer Method Biomed Eng 2014;30(3): 430-45.
12) Inthavong K, Ma J, Shang Y, Dong J, Chetty ASR, Tu J, et al. Geometry and airflow dynamics analysis in the nasal cavity during inhalation. Clin Biomech (Bristol, Avon) 2019;66:97-106.
13) Chung SK, Na Y. Dynamic characteristics of heat capacity of the human nasal cavity during a respiratory cycle. Respir Physiol Neurobiol 2021;290:103674.
14) Xiong GX, Zhan JM, Zuo KJ, Rong LW, Li JF, Xu G. Use of computational fluid dynamics to study the influence of the uncinate process on nasal airflow. J Laryngol Otol 2011;125(1):30-7.
15) Leong SC, Chen XB, Lee HP, Wang DY. A review of the implications of computational fluid dynamic studies on nasal airflow and physiology. Rhinology 2010;48(2):139-45.
16) Won TB, Cho SW, Sung MW, Paek SH, Chan S, Salisbury K, et al. Validation of a rhinologic virtual surgical simulator for performing a Draf 3 endoscopic frontal sinusotomy. Int Forum Allergy Rhinol 2019;9(8):910-7.
17) Abouali O, Keshavarzian E, Farhadi Ghalati P, Faramarzi A, Ahmadi G, Bagheri MH. Micro and nanoparticle deposition in human nasal passage pre and post virtual maxillary sinus endoscopic surgery. Respir Physiol Neurobiol 2012;181(3):335-45.
18) Lindemann J, Keck T, Wiesmiller K, Sander B, Brambs HJ, Rettinger G, et al. A numerical simulation of intranasal air temperature during inspiration. Laryngoscope 2004;114(6):1037-41.
19) International Commission on Radiological Protection. Human respiratory tract model for radiological protection. Ann ICRP 1994;24(1-3): 1-482.
20) Costa ML, Psaltis AJ, Nayak JV, Hwang PH. Long-term outcomes of endoscopic maxillary mega-antrostomy for refractory chronic maxillary sinusitis. Int Forum Allergy Rhinol 2015;5(1):60-5.
21) Cho DY, Hwang PH. Results of endoscopic maxillary mega-antrostomy in recalcitrant maxillary sinusitis. Am J Rhinol 2008;22(6):658-62.
22) Kennedy DW, Shaalan H. Reevaluation of maxillary sinus surgery: experimental study in rabbits. Ann Otol Rhinol Laryngol 1989;98(11): 901-6.
23) Suzuki M, Nakamura Y, Yokota M, Ozaki S, Murakami S. Modified transnasal endoscopic medial maxillectomy through prelacrimal duct approach. Laryngoscope 2017;127(10):2205-9.
24) Lundberg JO. Nitric oxide and the paranasal sinuses. Anat Rec (Hoboken) 2008;291(11):1479-84.
25) Zhang J, Sun Y, Liu M, Sun C, Tian L. Predictive and diagnostic value of fractional exhaled nitric oxide in patients with chronic rhinosinusitis. Med Sci Monit 2019;25:150-6.
26) Kirihene RK, Rees G, Wormald PJ. The influence of the size of the maxillary sinus ostium on the nasal and sinus nitric oxide levels. Am J Rhinol 2002;16(5):261-4.
27) Saibene AM, Felisati G, Pipolo C, Bulfamante AM, Quadrio M, Covello V. Partial preservation of the inferior turbinate in endoscopic medial maxillectomy: a computational fluid dynamics study. Am J Rhinol Allergy 2020;34(3):409-16.
28) Eccles R, Jones AS. The effect of menthol on nasal resistance to air flow. J Laryngol Otol 1983;97(8):705-9.
29) Jones AS, Crosher R, Wight RG, Lancer JM, Beckingham E. The effect of local anaesthesia of the nasal vestibule on nasal sensation of airflow and nasal resistance. Clin Otolaryngol Allied Sci 1987;12(6): 461-4.
30) Malik J, Spector BM, Wu Z, Markley J, Zhao S, Otto BA, et al. Evidence of nasal cooling and sensory impairments driving patient symptoms with septal deviation. Laryngoscope 2022;132(3):509-17.

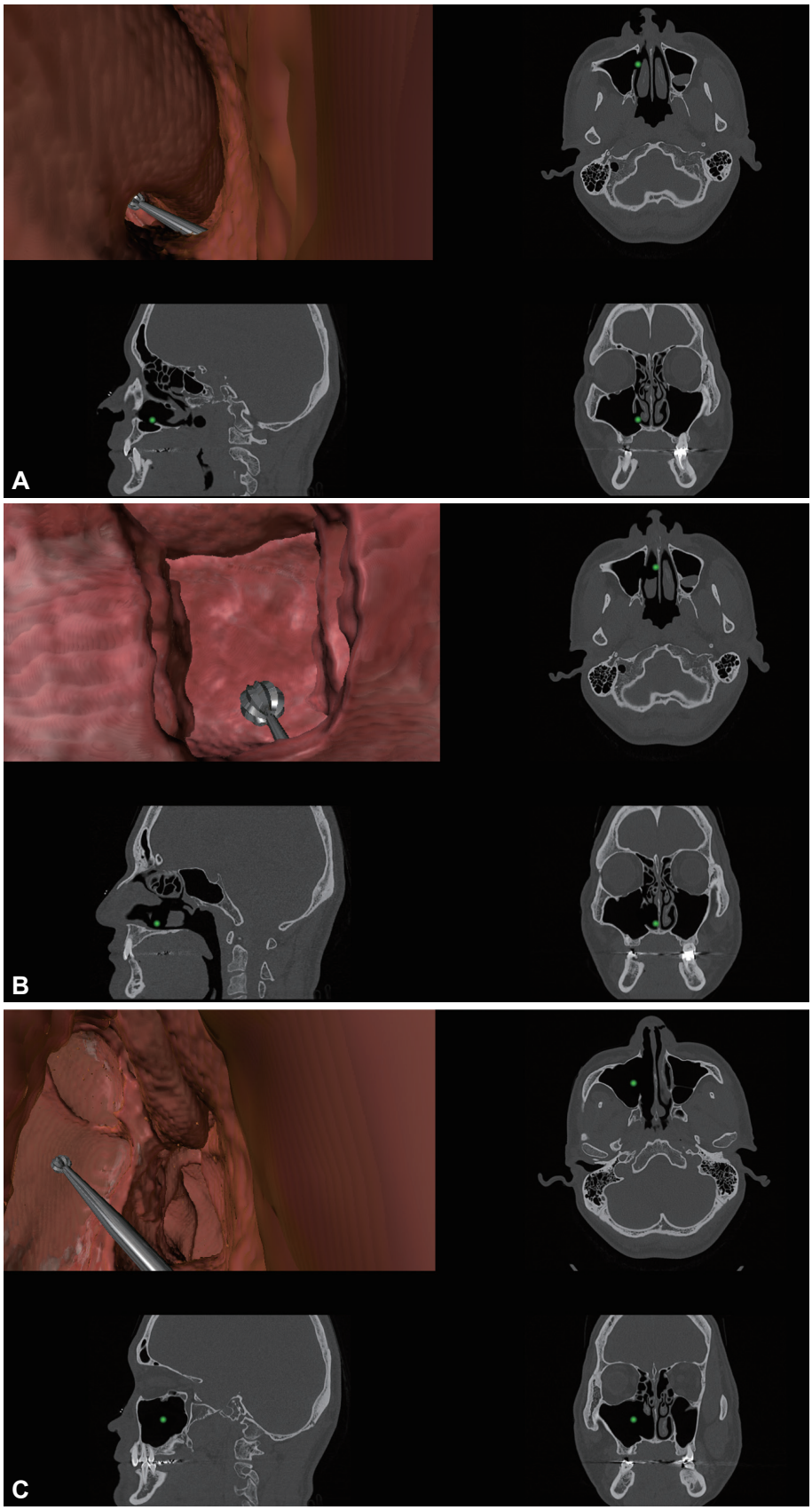

Supplementary Fig. 1. Virtual operation procedure scene using virtual simulator platform software. A: An endoscopic view after a virtual operation involving MMA+IMA is shown. The green dots on the axial, sagittal, and coronal images of CT represent the site of the end of the drill that is placed in the endoscopic view. The drill is placed near the IMA site. B: An endoscopic view after a virtual operation involving MEGA is shown. The green dots on the axial, sagittal, and coronal images of CT represent the site of the end of the drill that is placed in the endoscopic view. The drill is placed near the partial inferior turbinectomy site. The endoscopic view is more widely enlarged. C: The endoscopic view after a virtual operation involving EMM is shown. The green dots on the axial, sagittal, and coronal images of CT represent the site of the end of the drill that is placed in the endoscopic view. The drill is placed almost in the maxillary sinus. MMA, middle meatal antrostomy; IMA, inferior meatal antrostomy; CT, computed tomography; MEGA, mega-antrostomy; EMM, endoscopic medial maxillectomy.

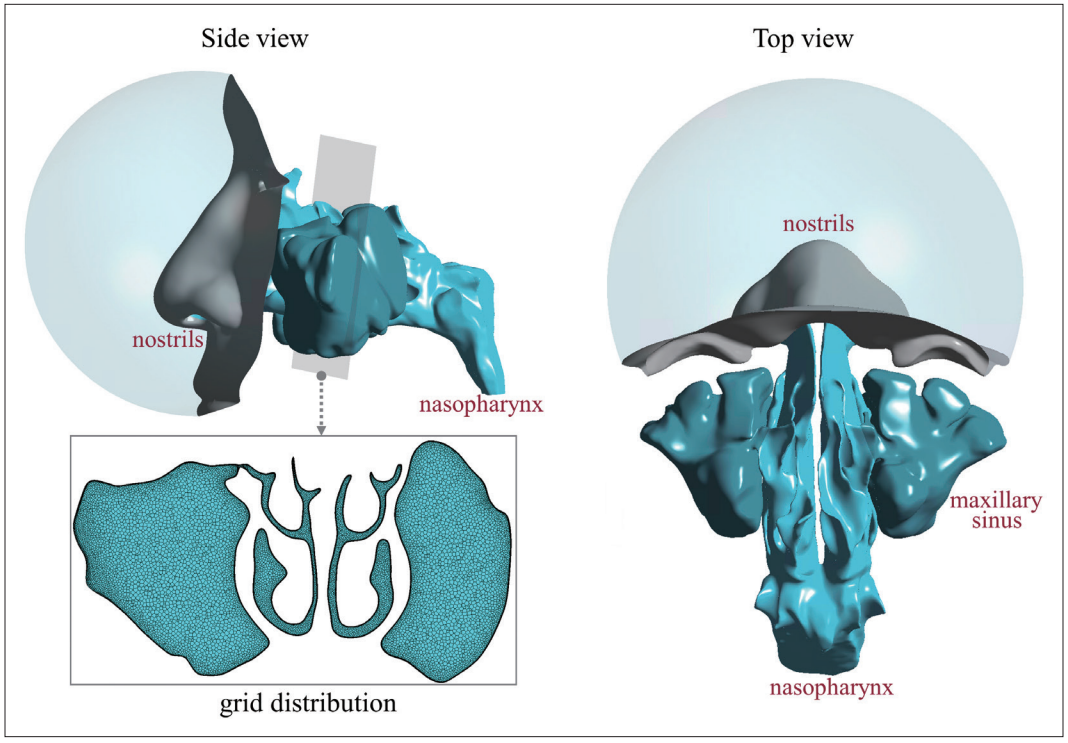

Supplementary Fig. 2. Numerical model of the nasal cavity constructed using CT scans of the baseline model. A 3-dimensional computational volume model was segmented from baseline CT. Approximately 5.2–5.3 million mesh elements consisting of both prism layers and the polyhedral mesh were generated. The mesh distribution in one representative plane is shown. CT, computed tomography.

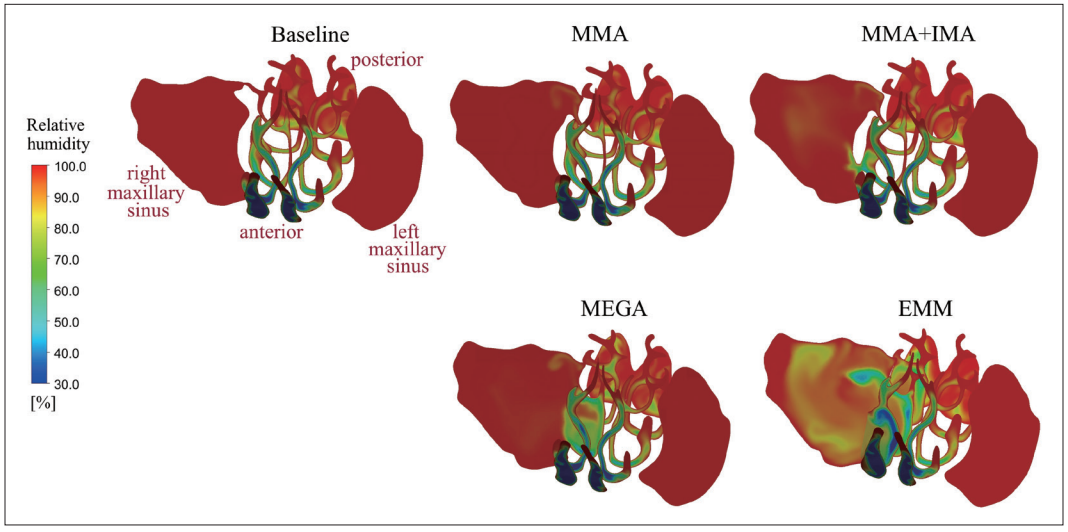

Supplementary Fig. 3. Comparison of relative humidity distributions in five representative coronal planes. The bilateral relative humidity is shown on five representative planes from the anterior part to the posterior part. In the baseline model, the relative humidity inside the MS was almost undisturbed. In the MMA, MMA+IMA, and MEGA models, the average relative humidity of the right MS was over 97% (i.e., 99.7%, 97.4%, and 98.4%, respectively). In the EMM model, the entire volume of the MS was affected by the airflow penetration, and the resulting spatial average of the relative humidity in the right MS dropped to 89.8%. MMA, middle meatal antrostomy; IMA, inferior meatal antrostomy; MEGA, mega-antrostomy; EMM, endoscopic medial maxillectomy; MS, maxillary sinus.

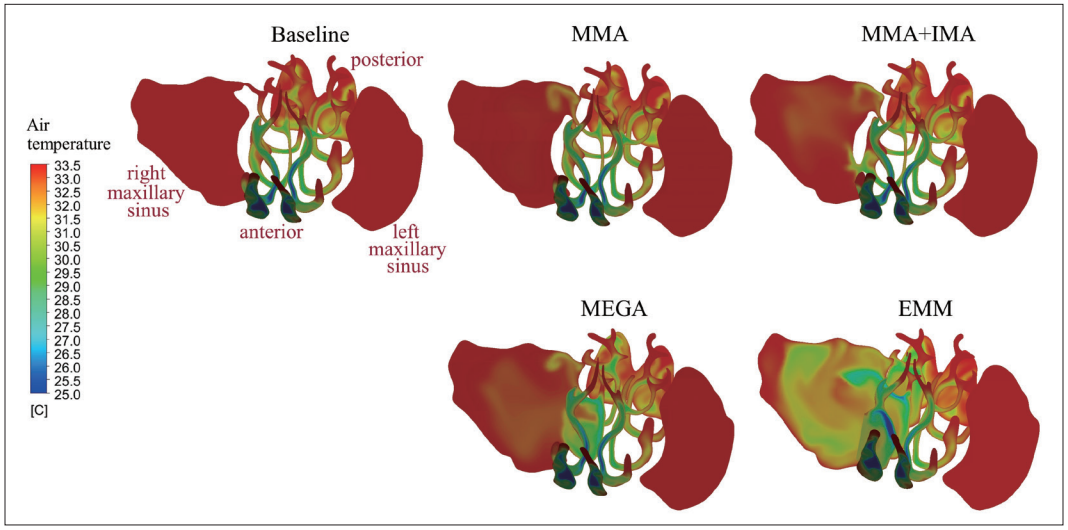

Supplementary Fig. 4. Comparison of air temperature distributions in five representative coronal planes. The bilateral relative air temperature is shown on five representative planes from the anterior part to the posterior part. The behaviors of the air temperature fields were similar to those of the relative humidity fields. In the MMA, MMA+IMA, and MEGA models, the average temperature was maintained over 33°C in the right MS (i.e., 33.3°C, 33.1°C, and 33.0°C, respectively). However, in the EMM model, the average temperature of the right MS dropped to 31.6°C. MMA, middle meatal antrostomy; IMA, inferior meatal antrostomy; MEGA, mega-antrostomy; MS, maxillary sinus; EMM, endoscopic medial maxillectomy.